Molecular Interaction Modulating Ruddlesden-Popper Tin-based Perovskite Crystallization

Han Pan*[a], Yong Zheng [a], Wenqing He [a], Wenxing Yang*[a], Xiu Gong [b], Xiaodong Liu [c], Qiang Wei [d], Yan Liu [e], Yan Shen [f] and Mingkui Wang *[f]

[a] School of Physics and Optoelectronic Engineering, Yangtze University, Jingzhou 434023, China

[b] College of Physics, Guizhou Province Key Laboratory for Photoelectrics Technology and Application, Guizhou University, Guiyang 550025, China

[c] College of Chemistry and Environmental Engineering, Yangtze University, Jingzhou 434023, China

[d] State Key Laboratory of Heavy Oil Processing, China University of Petroleum, Beijing 102249, China

[e] School of Physics and Optoelectronic Engineering, Ludong University, Yantai, 264025, China

[f] Wuhan National Laboratory for Optoelectronics, School of Optoelectronic Science and Engineering, Huazhong University of Science and Technology, Wuhan 430074, China

Experimental Section

SnI_2 (99.999%), hydroiodic acid (57 wt.% in H_2O, distilled, stabilized, 99.95%), hypophosphorous acid solution (50 wt.% in H_2O) and formamidinium iodide (≥99%, anhydrous) were purchased from Sigma-Aldrich and used as received. Benzylamine (99%) and 2-Thiophenemethylamine (97%) were purchased from Aladdin and used as received.

Synthesis of BEI and THI: hydroiodic acid (12.3 g, 0.055 mol) reacted with benzylamine (5.3 g, 0.05 mol.) for 2 hours under ice bath. The crude product was separated out by evaporating the solvent under reduced pressure. White crystals were obtained after washed with diethyl ether, recrystallized in ethanol and drying at 60 °C overnight in a vacuum. THI was prepared using the same method, only changed the benzylamine to 2-Thiophenemethylamine

The perovskite precursor solutions were prepared by mixing BEI or THI, FAI, SnI_2 and SnF_2 in anhydrous in DMF and DMSO (volume ratio is 4:1) with a molar ratio of 2:3:4:0.1. The concentration of $(BE)_2FA_3Sn_4I_{17}$ and $(TH)_2FA_3Sn_4I_{17}$ is 0.1 M. The mixture solutions were stirred for 2h in N_2 glove box.

Device fabrication

The ITO glass was sequentially cleaned with detergent, deionized water, acetone and ethanol, and then treated in UV-ozone for 30 min. A 40 nm thick PEDOT:PSS (Baytron PVP Al 4083) was spin-coated onto the ITO substrate at 4500 rpm for 40 s and annealed at 140 °C for 10 min in air. After perovskite films were spin-coated at 4000 rpm for 60 s and then annealed on 60 °C for 10 seconds and post on 100 °C for 10 minutes, $PC_{61}BM$ (20 $mg \cdot mL^{-1}$ in chlorobenzene) and BCP (0.5 $mg \cdot mL^{-1}$ in isopropanol) were sequentially coated at 2000 rpm for 40 s and 4000 rpm for 40 s, respectively. Finally, 100 nm Ag was deposited by thermal evaporation.

Characterization

XRD measurements were performed with a Shimadzu XRD-6100 diffractometer with Cu Kα radiation. The surface morphology of films were characterized with FEI Nova Nano SEM 450. The crystallization process of perovskite films fabricated from the solutions were recorded by optical microscope (Olympus BX51). Visible absorption

spectra were recorded using a PerkinElmer Lambda1050 spectrophotometer. The steady-state photoluminescence (PL) spectrum was measured using Horiba Jobin Yvon system with an excitation laser beam at 532 nm and a repetition rate of 76 MHz. The time-resolved luminescence decays were obtained with time-correlated single photo counting system (PicoHarp 300, PicoQuant GmbH). The excitation light source was Ti:Sapphire laser (Mira 900, Coherent; 76 MHz, 130 fs). The photocurrent-voltage (J-V) characteristics of Cl-$PEA_2MA_3Pb_4I_{13}$ solar cells were obtained by a Keithley model 2400 digital source meter. A xenon light source solar simulator (450 W, Oriel, model 9119) with AM 1.5G filter (Oriel, model 91192) was used to give an irradiance of 100 mW cm^{-2} at the surface of the solar cells. The incident photon conversion efficiency (IPCE) measurement was obtained with alternating current (AC) model (130 Hz). The dynamic light scattering and zeta potential measurement of the perovskite precursor solutions were measured using Brookhaven 90Plus Particle Size and PALS Zeta Potential Analyzer.

Determination of aggregation rate

The initial aggregation rate constant (k) of colloids is determined by the initial increase of the hydrodynamic radius D_h with time t in the period from aggregation initiation (t_0) to the time when D_h reached 1.25 D_h: [1, 2]

$$k \propto \frac{1}{N_0}\left(\frac{dD_h(t)}{dt}\right)_{t\to 0} \quad (1)$$

where N_0 is the initial concentration of colloidal solutions. The value of $dD_h(t)/dt$ was obtained through a linear least-squares regression analysis.

Measure

Density functional theory (DFT) calculation was performed by DMol[3] code of Materials Studio. The generalized gradient approximation of revised-Perdew-Burke-Ernzerhof (GGA-RPBE) function and Grimme of DFT-D dispersion correction were used to treat all the energy changes[3, 4]. The core treatment was effective core potentials (ECP) and the basis set was DNP v4.4. The k-point was set as 3 × 3 × 1 and the size of

vacuum region was 20 Å[5]. The detailed calculation parameters were reported in our previous studies[6]. The typical perovskite framework contained 23 Iodine atoms and 10 Tin atoms as well as 4 FA molecules in the middle layer, as shown in Fig.1. The lattice parameters of one perovskite unit were a=b=8.8379 Å after optimization. During calculation, the bottom and the middle layer was fixed and the top layer was relaxed to simulate the constraint.

The adsorption energy of molecules on perovskite surface was defined as Eq. (2).

$$E_{ads} = E_{cat+mol} - E_{cat} - E_{mol} \quad (2)$$

Where $E_{cat+mol}$ is the energy of adsorbed molecule on catalyst surface, E_{cat} is the energy of bare catalyst surface and E_{mol} is the energy of the molecule in gas phase.

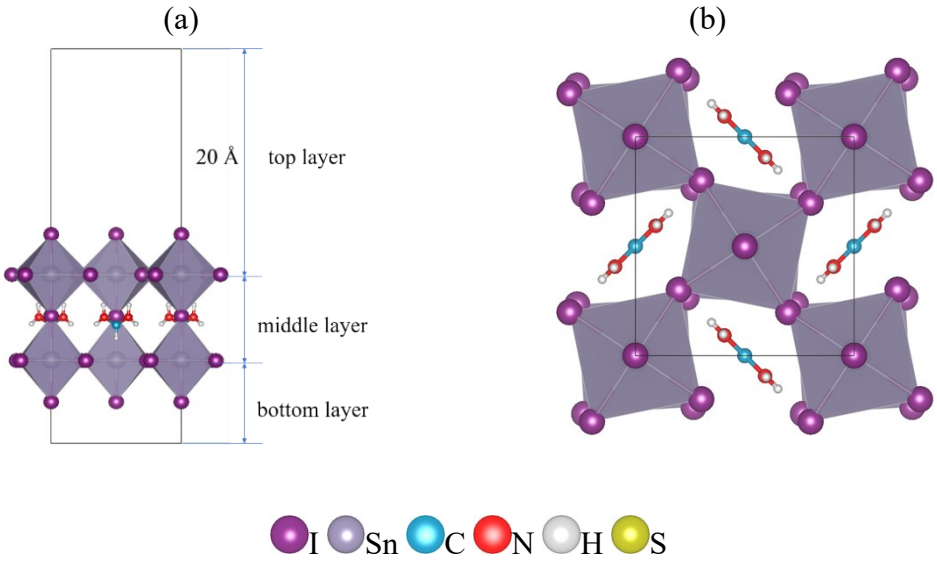

Figure S1. Diagram of the perovskite model, (a) side view, (b) top view.

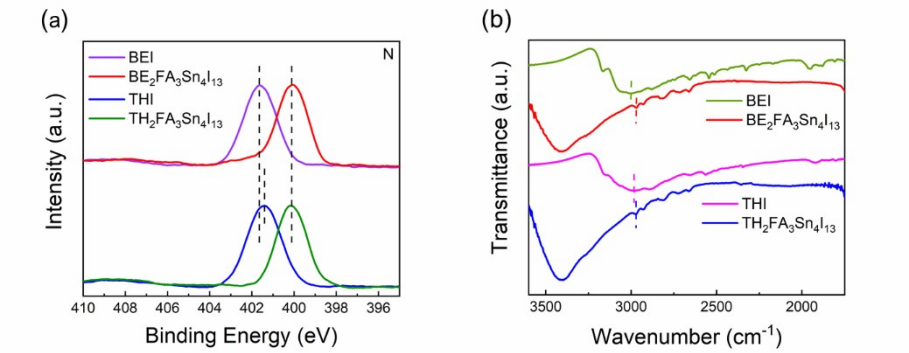

Figure S2. (a) X-ray photoelectron spectroscopy (XPS) spectrum of N 1s and (b) Fourier transform infrared (FT-IR) spectrum for BEI, $BE_2FA_3Sn_4I_{13}$, THI and $TH_2FA_3Sn_4I_{13}$. Dotted lines present NH_3^+ stretching vibration.

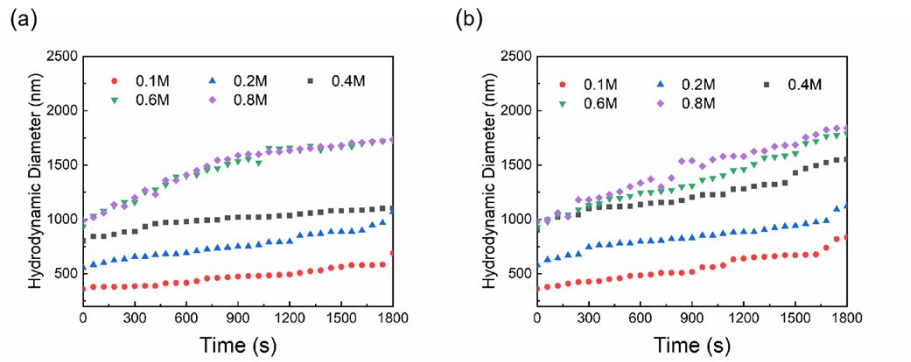

Figure S3. Aggregation profiles of (a) $BE_2FA_3Sn_4I_{13}$-based and (b) $TH_2FA_3Sn_4I_{13}$-based colloids at selected concentrations of 0.1, 0.2, 0.4, 0.6, and 0.8 mol.

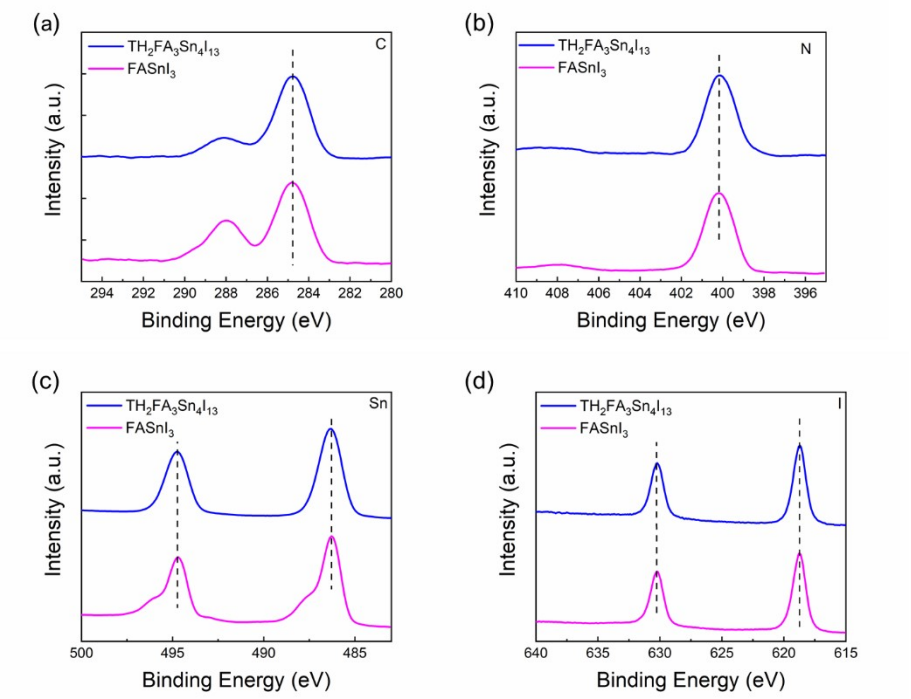

Figure S4. XPS spectra of (a) C 1s, (b) N 1s, (c) Sn 3d and (d) I 3d for $TH_2FA_3Sn_4I_{13}$ and $FASnI_3$ perovskites films.

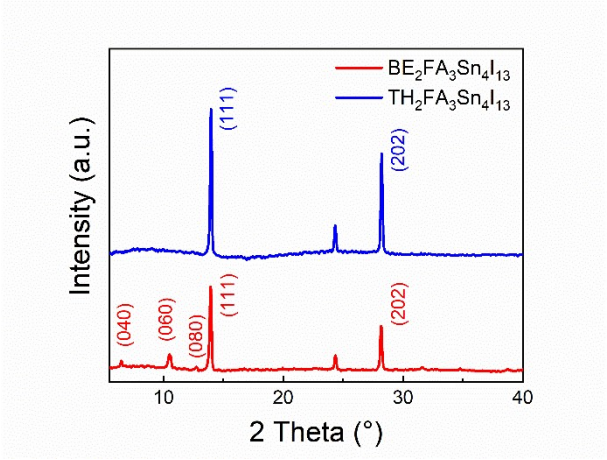

Figure S5. XRD patterns of $BE_2FA_3Sn_4I_{13}$-based and $TH_2FA_3Sn_4I_{13}$-based perovskite films.

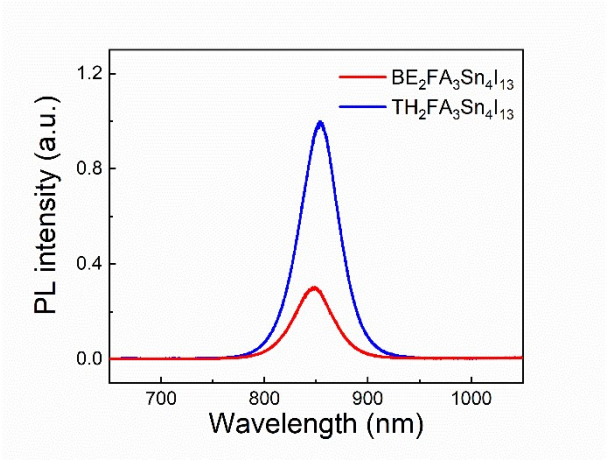

Figure S6. Steady-state PL spectra of $BE_2FA_3Sn_4I_{13}$-based and $TH_2FA_3Sn_4I_{13}$-based perovskite films.

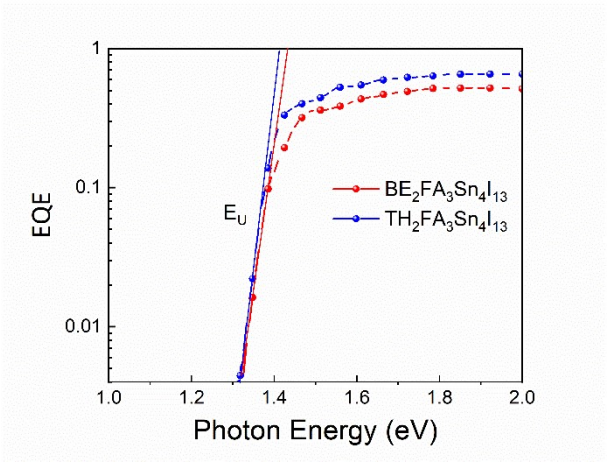

Figure S7. Semi-log plot of EQE values versus photon energy of the $BE_2FA_3Sn_4I_{13}$-based and $TH_2FA_3Sn_4I_{13}$-based devices.

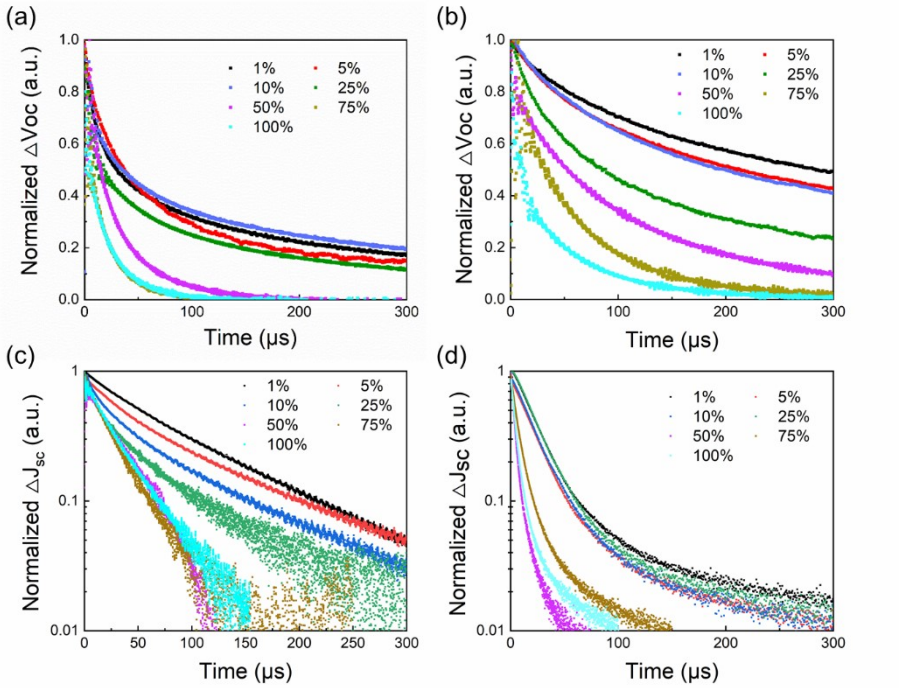

Figure S8. Transient photovoltage of a) $BE_2FA_3Sn_4I_{13}$-based and b) $TH_2FA_3Sn_4I_{13}$-based devices under varying light intensity. Transient photocurrent of c) $BE_2FA_3Sn_4I_{13}$-based and d) $TH_2FA_3Sn_4I_{13}$-based devices under varying light intensity.

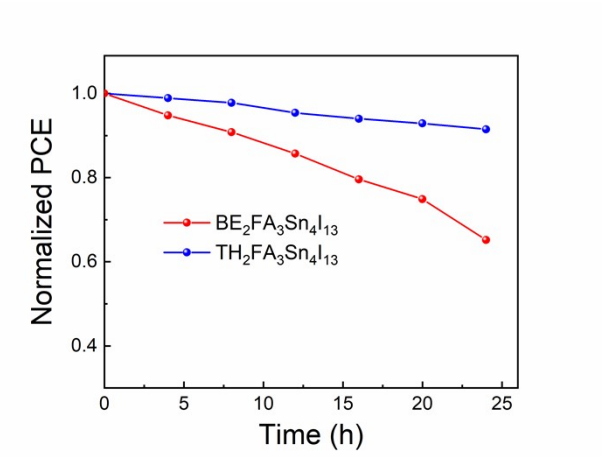

Figure S9. Normalized PCEs versus time for the $BE_2FA_3Sn_4I_{13}$-based and $TH_2FA_3Sn_4I_{13}$-based devices.

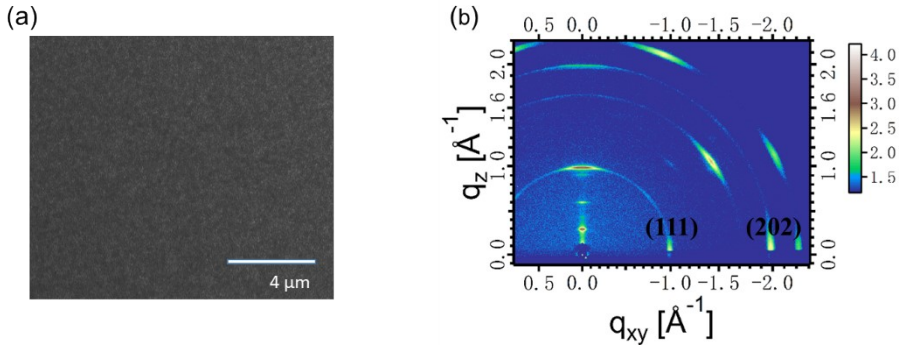

Figure S10. (a) The top-view SEM images and (b) GIWAXS of $FU_2FA_3Sn_4I_{13}$-based film.

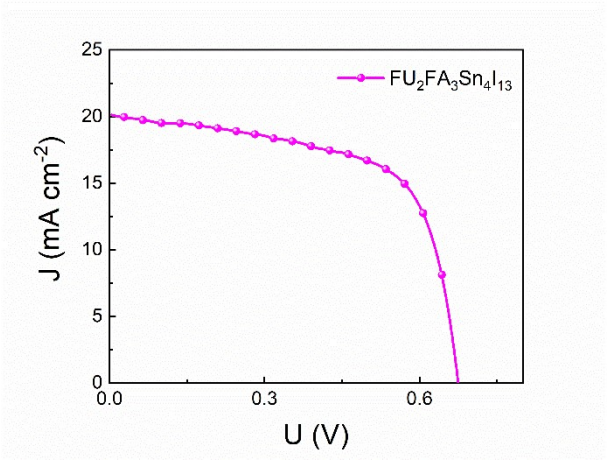

Figure S11. The photocurrent J-V curve of $FU_2FA_3Sn_4I_{13}$-based device.

Table S1. The photovoltaic parameters of the $BE_2FA_3Sn_4I_{13}$-based and $TH_2FA_3Sn_4I_{13}$-based devices with different scan directions.

Device	Scan direction	*V*oc (V)	*J*sc (mA cm^{-2})	FF (%)	PCE (%)
$BE_2FA_3Sn_4I_{13}$	RS	0.53	14.88	51.2	4.04
	FS	0.51	14.34	47.2	3.45
$TH_2FA_3Sn_4I_{13}$	RS	0.68	20.94	63.4	9.03
	FS	0.67	20.87	61.2	8.64

References

1. K. L. Chen and M. Elimelech, *Langmuir*, 2006, **22**, 10994-11001.
2. W. Yang, J. Shang, P. Sharma, B. Li, K. Liu and M. Flury, *Sci. Total Environ.*, 2019, **658**, 1306-1315.
3. B. Hammer, L. B. Hansen and J. K. Nørskov, *Physical Review B*, 1999, **59**, 7413.
4. S. Grimme, *WIREs Computational Molecular Science*, 2011, **1**, 211-228.
5. H. Monkhorst and J. Pack, *Phys. Rev. B*, 1976, **13**, 5188-5192.
6. Q. Wei, X. Liu, Y. Zhou, Z. Xu, P. Zhang and D. Liu, *Catal. Today*, 2020, **353**, 39-46.